# REPORT DOCUMENTATION PAGE

Form Approved
OMB NO. 0704-0188

Public reporting burden for this collection of information is estimated to average 1 hour per response, including the time for reviewing instructions, searching existing data sources, gathering and maintaining the data needed, and completing and reviewing the collection of information. Send comment regarding this burden estimates or any other aspect of this collection of information, including suggestions for reducing this burden, to Washington Headquarters Services, Directorate for information Operations and Reports, 1215 Jefferson Davis Highway, Suite 1204, Arlington, VA 22202-4302, and to the Office of Management and Budget, Paperwork Reduction Project (0704-0188), Washington, DC 20503.

1. AGENCY USE ONLY (Leave blank)	2. REPORT DATE	3. REPORT TYPE AND DATES COVERED
		Reprint

4. TITLE AND SUBTITLE

Modeling Space Charge in Alternating-Current Thin-Film Electroluminescent Devices Using a Single-Sheet Charge Model

5. FUNDING NUMBERS

DAAH04-94-G-0324

6. AUTHOR(S)

P.D. Keir, W.M. Ang, J.F. Wager

7. PERFORMING ORGANIZATION NAMES(S) AND ADDRESS(ES)

Oregon State University
Department of Electrical and Computer Engineering
Corvallis, OR   97331-3211

8. PERFORMING ORGANIZATION REPORT NUMBER

9. SPONSORING / MONITORING AGENCY NAME(S) AND ADDRESS(ES)

U.S. Army Research Office
P.O. Box 12211
Research Triangle Park, NC 27709-2211

10. SPONSORING / MONITORING AGENCY REPORT NUMBER

ARO 32693.1-PH

11. SUPPLEMENTARY NOTES

The views, opinions and/or findings contained in this report are those of the author(s) and should not be construed as an official Department of the Army position, policy or decision, unless so designated by other documentation.

12a. DISTRIBUTION / AVAILABILITY STATEMENT

Approved for public release; distribution unlimited.

12 b. DISTRIBUTION CODE

19960524 112

13. ABSTRACT (Maximum 200 words)

A simulation of alternating-current thin-film electroluminescent device operation with positive space charge present in the phosphor layer of the device is presented. The simulation is based on modeling the space-charge distribution using a single-sheet charge model. The simulation is performed for two cases of space-charge creation: by impact ionization of deep levels in the phosphor or by field emission from traps in the phosphor. Results of the simulation show that space-charge creation by either mechanism is capable of causing overshoot in both capacitance-voltage and internal charge-phosphor field (Q-F_p) plots. © 1995 American Institute of Physics.

14. SUBJECT TERMS

Electroluminescence, Sheet-Charge, ACTFEL, Space-Charge

15. NUMBER IF PAGES

16. PRICE CODE

17. SECURITY CLASSIFICATION OR REPORT	18. SECURITY CLASSIFICATION OF THIS PAGE	19. SECURITY CLASSIFICATION OF ABSTRACT	20. LIMITATION OF ABSTRACT
UNCLASSIFIED	UNCLASSIFIED	UNCLASSIFIED	UL

DISCLAIMER NOTICE
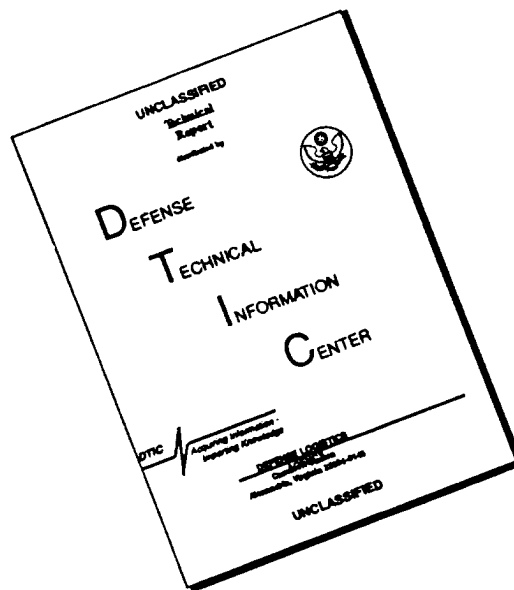
THIS DOCUMENT IS BEST QUALITY AVAILABLE. THE COPY FURNISHED TO DTIC CONTAINED A SIGNIFICANT NUMBER OF PAGES WHICH DO NOT REPRODUCE LEGIBLY.

Modeling space charge in alternating-current thin-film electroluminescent devices using a single-sheet charge model

P. D. Keir, W. M. Ang, and J. F. Wager
Center for Advanced Materials Research, Department of Electrical and Computer Engineering,
Oregon State University, Corvallis, Oregon 97331-3211

A simulation of alternating-current thin-film electroluminescent device operation with positive space charge present in the phosphor layer of the device is presented. The simulation is based on modeling the space-charge distribution using a single-sheet charge model. The simulation is performed for two cases of space-charge creation: by impact ionization of deep levels in the phosphor or by field emission from traps in the phosphor. Results of the simulation show that space-charge creation by either mechanism is capable of causing overshoot in both capacitance-voltage and internal charge-phosphor field (Q-F_p) plots. © *1995 American Institute of Physics.*

I. INTRODUCTION

A common simplifying assumption in many previously developed alternating-current thin-film electroluminescent (ACTFEL) device models is that the entire phosphor layer of the device is a constant field region.[1-5] The assumption of constant phosphor field implies that bulk space charge does not exist in the phosphor layer. In modeling ZnS:Mn devices grown by evaporation, the results obtained under the assumption of a constant phosphor field match the measured results very well.[6,7] However, with the advent of alternative phosphor materials and methods of fabrication, certain effects have been experimentally observed that cannot be described using a constant phosphor field model.

The effects commonly observed in experimental measurements of ACTFEL devices that are not consistent with the constant phosphor field model are brightness-voltage (B-V) hysteresis,[2,8-10] negative differential resistance,[11,12] capacitance-voltage (C-V) overshoot,[13,14] and internal charge-phosphor field (Q-F_p) overshoot.[13-15] Other researchers have developed numerical models to account for the existence of space charge in the phosphor layer of an ACTFEL device, primarily focusing on the issues of B-V hysteresis[9,16-18] and negative differential resistance.[11,12] In contrast, the work presented herein is concerned with modeling both C-V and Q-F_p overshoot using a single-sheet charge model[7] to account for space charge in the phosphor. In particular, effects seen in ZnS:Mn devices grown by atomic layer epitaxy (ALE) are considered. The information gained from simulation of the single-sheet charge model is then used to aid in the interpretation of laboratory measurements of ACTFEL devices exhibiting space-charge related effects.

The two distinguishing characteristics of the work presented herein is the utilization of a single-sheet charge model and the application of this modeling towards obtaining an understanding of C-V and Q-F_p overshoot. The single-sheet charge ACTFEL device model is chosen over distributed models[11,12,19] for two primary reasons. First, the lumping of the space-charge distribution into a single sheet greatly simplifies the problems associated with the presence of space charge in the phosphor layer. Second, the highly polarity-

dependent electrical characteristics of ALE ZnS:Mn devices being modeled suggest that the space-charge distribution is concentrated near the edges of the phosphor layer, rather than evenly distributed across the width of the phosphor layer.

It should also be noted that most of the previous research performed on modeling space-charge-related effects of ACT-FEL devices has assumed the method of space-charge creation is the trapping of holes generated by band-to-band impact ionization processes.[9,12,17,19] However, Yang *et al.* provide experimental evidence that hot-electron impact ionization of deep levels is more likely to cause hysteresis than hole trapping.[10] Therefore, the focus of the modeling in this paper is towards modeling space-charge creation as due to either impact ionization of deep levels or field emission of electrons from bulk traps.

II. SINGLE-SHEET CHARGE MODEL

A. Single-sheet charge model quasistatics

The single-sheet charge model for an ACTFEL device models a space-charge distribution in the phosphor layer as a sheet of charge at a single, arbitrary location within the phosphor layer.[7] The general form of the single-sheet charge model is depicted in Fig. 1. In Fig. 1, i_1 and i_2 refer to the ACTFEL insulator layers, the subscript "sc" refers to the single-sheet charge layer, and p_1 and p_2 refer to the two different regions of the phosphor within which the electric field may be different because of the existence of the space-charge layer. The labels f, d, and q refer, respectively, to the electric field, charge density, and thickness of the subscripted layers.

To develop an analytical description for the single-sheet charge model to be simulated, various basic principles are applied to derive a set of equations that describe the quasistatics of the model. This process begins by application of Kirchoff's voltage law to the structure of Fig. 1 to yield

$$d_{i1}f_{i1}(t) + d_s f_{p1}(t) + (d_p - d_s)f_{p2}(t) + d_{i2}f_{i2}(t) = -v_g(t). \tag{1}$$

Two things should be noted from the above equation and from Fig. 1. First, the sign convention of the electric field
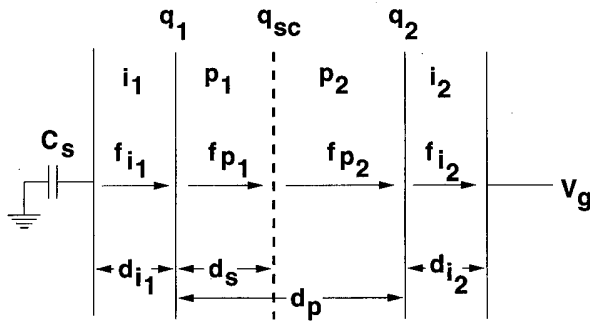
FIG. 1. Single-sheet charge model of an ACTFEL device.

terms in Eq. (1) is opposite the usual textbook convention for electric fields. This convention is adopted to stay consistent with the formulation presented by Bringuier[3] and other work based on the use of this convention.[13–15] Second, the external series capacitor C_s is neglected in formulating Eq. (1). This is a valid assumption because in laboratory measurements C_s is chosen to be large compared to the capacitance presented by the ACTFEL device. Next, Gauss' Law is applied to each of the charge interfaces to yield the following three equations:

$$c_{i1}d_{i1}f_{i1}(t) - c_p d_p f_{p1}(t) = -q_1(t), \tag{2}$$

$$c_p d_p [f_{p1}(t) - f_{p2}(t)] = -q_{sc}(t), \tag{3}$$

$$c_p d_p f_{p2}(t) - c_{i2}d_{i2}f_{i2}(t) = -q_2(t), \tag{4}$$

where the c terms represent the capacitance of the subscripted layer. Then, it is necessary to add an external equation that relates the charge on the initially cathodic electrode to the charge measured on a capacitor in series with the ACTFEL device. This equation represents the bridge between experimentally measurable information and the internal device physics. The external equation,

$$c_{i1}d_{i1}f_{i1}(t) = -q_e(t), \tag{5}$$

remains unchanged from the model presented by Bringuier that assumes no space-charge creation in the device.[3] Finally, invoking the necessity for charge balance inside the device, it is known that

$$q_1(t) + q_2(t) + q_{sc}(t) = 0. \tag{6}$$

The above six equations serve to completely describe all charge densities and fields in the single-sheet charge model. The scope of their utility will become evident throughout the development of the dynamic single-sheet charge model.

The first steps in the development of the dynamic single-sheet charge model are to perform several manipulations of Eqs. (1) through (6). First, adding Eqs. (2) through (4) and substituting Eq. (6) into the sum yields the following result:

$$c_{i1}d_{i1}f_{i1}(t) = c_{i2}d_{i2}f_{i2}(t). \tag{7}$$

Since $c_{i1}d_{i1}$ and $c_{i2}d_{i2}$ represent the dielectric permittivities of each respective insulator layer, it follows that the insulator fields divide according to the ratio of the dielectric constants of the respective insulating materials. Therefore, for ACTFEL devices with insulating layers of the same material and

thickness, $f_{i1}(t) = f_{i2}(t)$. Throughout the remainder of this article it is assumed that the device being modeled is fabricated such that both insulator layers are identical.

The next step towards obtaining the dynamic model for the evolution of the phosphor fields is to find expressions for both f_{p1} and f_{p2}. When Eqs. (2), (4), (5), and (7) are solved for f_{p1} and f_{p2}, respectively, the expressions

$$f_{p1}(t) = \frac{1}{c_p d_p}[q_1(t) - q_e(t)], \tag{8}$$

$$f_{p2}(t) = -\frac{1}{c_p d_p}[q_2(t) + q_e(t)] \tag{9}$$

are obtained. The significance of Eqs. (8) and (9) lies in the fact that expressions are obtained for $f_{p1}(t)$ and $f_{p2}(t)$ that depend exclusively on the values of the three charge variables, $q_1(t)$, $q_2(t)$, and $q_e(t)$.

B. The dynamics of the single-sheet charge model

To obtain the basis of the dynamic model, the expressions for f_{p1} and f_{p2} in Eqs. (8) and (9) are differentiated with respect to time. The resultant equations are the following pair of coupled, first-order differential equations:

$$\frac{\partial f_{p1}}{\partial t} = \frac{1}{c_p d_p}\left(\frac{\partial q_1}{\partial t} - \frac{\partial q_e}{\partial t}\right), \tag{10}$$

$$\frac{\partial f_{p2}}{\partial t} = -\frac{1}{c_p d_p}\left(\frac{\partial q_2}{\partial t} + \frac{\partial q_e}{\partial t}\right). \tag{11}$$

Next, when Eqs. (1) through (6) are self-consistently solved for q_e in terms of q_1, q_{sc}, and v_g, and the result is differentiated with respect to time,

$$\frac{\partial q_e}{\partial t} = \frac{c_i}{c_i + c_p}\left[\frac{\partial q_1}{\partial t} + \left(1 - \frac{d_s}{d_p}\right)\frac{\partial q_{sc}}{\partial t}\right] + c_t\frac{\partial v_g}{\partial t} \tag{12}$$

is obtained. The expression for $\partial q_e/\partial t$ given by Eq. (12) and the charge neutrality condition given by Eq. (6) are then substituted into Eqs. (10) and (11) to give expressions for $\partial f_{p1}/\partial t$ and $\partial f_{p2}/\partial t$ in terms of the time derivatives of the charge on each interface. The equations

$$\frac{\partial f_{p1}}{\partial t} = \frac{1}{c_p d_p}\left\{\frac{\partial q_1}{\partial t} - \left(\frac{c_i}{c_i + c_p}\right)\left[\frac{\partial q_1}{\partial t} + \left(1 - \frac{d_s}{d_p}\right)\frac{\partial q_{sc}}{\partial t}\right]\right.$$
$$\left. + c_t\frac{\partial v_g}{\partial t}\right\}, \tag{13}$$

$$\frac{\partial f_{p2}}{\partial t} = -\frac{1}{c_p d_p}\left\{\frac{\partial q_2}{\partial t} - \left(\frac{c_i}{c_i + c_p}\right)\left[\frac{\partial q_2}{\partial t} + \left(\frac{d_s}{d_p}\right)\frac{\partial q_{sc}}{\partial t}\right]\right.$$
$$\left. + c_t\frac{\partial v_g}{\partial t}\right\} \tag{14}$$

result. The above pair of differential equations is complete in that it describes the dynamics of the phosphor fields in terms of the three internal current density terms, $\partial q_1/\partial t$, $\partial q_2/\partial t$, and $\partial q_{sc}/\partial t$ along with the external voltage slew rate term, $\partial v_g/\partial t$. To complete the dynamic model, it is necessary to develop expressions for $\partial q_1/\partial t$, $\partial q_2/\partial t$, and $\partial q_{sc}/\partial t$. To de-
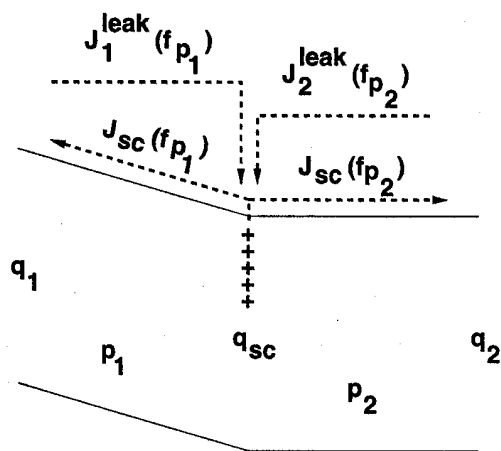
FIG. 2. Energy band diagram depicting the four space-charge current components.

FIG. 3. Energy band diagram depicting the current components of interface 1.

velop expressions for these three terms, it is first necessary to examine the situation at each charge interface more closely.

The first interface charge to consider is the sheet of space charge located at some arbitrary location in the phosphor bulk. The space-charge layer is depicted in Fig. 2 in an energy band diagram of the phosphor layer of the ACTFEL device. As seen in Fig. 2, the space-charge layer can emit electrons to either interface 1 or interface 2, depending on the field polarity in the phosphor layer. Also, the space-charge layer can trap electrons emitted from either interface 1 or interface 2. Each of the electron emission or reception events described above now must be converted to equation form to describe the time derivative of q_{sc}. To accomplish this, usual current conventions are employed; i.e., an electron emitting interface corresponds to a positive current into the interface in question, whereas a receiving interface corresponds to a negative current into the interface in question. Next, the field dependencies for electron emission need to be deduced. It is seen in Fig. 2 that both the emission of electrons from interface 1 to the space-charge layer and the emission of electrons from the space-charge layer to interface 1 are controlled by the field magnitude and polarity in phosphor region 1 (p_1). Similarly, electron emission to and from interface 2 is controlled by the field magnitude and polarity in phosphor region 2 (p_2). Finally, from the above considerations, the equation that is sought emerges,

$$\frac{\partial q_{sc}}{\partial t} = J_{sc}(f_{p1}) + J_{sc}(f_{p2}) - J_1^{leak}(f_{p1}) - J_2^{leak}(f_{p2}), \quad (15)$$

where J terms represent current densities from the subscripted emitting interface. It should be noted that the superscripts on the latter two terms in Eq. (15) represent the current emitted by the subscripted semiconductor-insulator interface that annihilates positive space charge. This current is denoted J^{leak} because it is standard to call charge emitted during the interpulse interval leakage charge,[13-15] and space charge is mostly annihilated during the low-field portion of the interpulse interval.

Continuing the same approach outlined above, Fig. 3 can be employed to produce a similar expression for $\partial q_1/\partial t$.
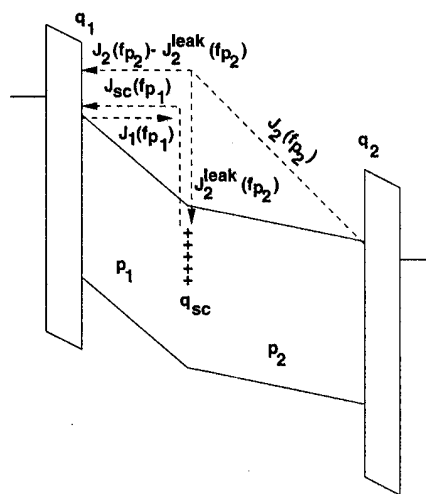
First, with the correct field polarity in the phosphor, electrons are emitted from interface 1. Then, with the opposite field polarity, electrons are emitted by the space-charge layer and received by interface 1. Also, concomitant with the space-charge emission, electrons are emitted from interface 2. However, some of these electrons are captured by the space-charge layer and never reach interface 1. Therefore, the superscript term from the development of the expression for $\partial q_{sc}/\partial t$ is the term that accounts for this. The total current reaching interface 1 is then the difference between J_2 and J_2^{leak}. This is shown pictorially in Fig. 3. Finally, the expression for $\partial q_1/\partial t$ is

$$\frac{\partial q_1}{\partial t} = J_1(f_{p1}) - J_2(f_{p2}) - J_{sc}(f_{p1}) + J_2^{leak}(f_{p2}), \quad (16)$$

where the J terms again represent emission from the subscripted interface. The J_{sc} and J_2^{leak} are the same terms used in the development of the expression for $\partial q_{sc}/\partial t$.

To complete the set of expressions for substitution into Eqs. (13) and (14), a similar expression for $\partial q_2/\partial t$ must be developed next. The figure of interest for electron emission and reception by interface 2 is Fig. 4. The development of this expression exactly parallels the development of the expression for $\partial q_1/\partial t$, so the details will be omitted. The desired expression is

$$\frac{\partial q_2}{\partial t} = J_2(f_{p2}) - J_1(f_{p1}) - J_{sc}(f_{p2}) + J_1^{leak}(f_{p1}). \quad (17)$$

Equations (15) through (17) generated above comprise the complete set of equations necessary for substitution into Eqs. (13) and (14).

III. ELECTRON EMISSION

To complete the simulation model, expressions must be developed that describe each of the current density terms in Eqs. (15) through (17). The approach to accomplishment of this goal is to first examine electron emission from the insulator-phosphor interfaces. Then, once this is established,
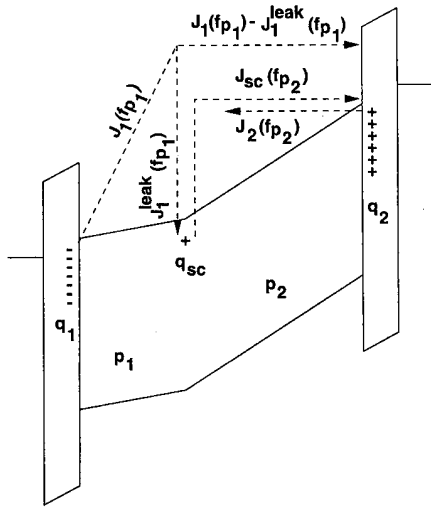
Keir, Ang, and Wager

FIG. 4. Energy band diagram depicting the current components of interface 2.

space-charge creation is examined for both the case of creation by field emission and of creation by impact ionization of deep levels. Finally, band-to-band impact ionization is considered. It should be noted that both interfaces and the space-charge layer are assumed to be discrete traps.

A. Insulator-semiconductor interfaces

Emission rates from the insulator-phosphor interface are controlled by both the field in the phosphor layer adjacent to the interface of interest and the ambient temperature. At low phosphor fields, phonon-assisted tunneling (PAT) and thermal emission (thermal) of carriers may be important mechanisms for carrier emission.[7] At high fields, the dominant mechanism for electron emission is by pure tunnel (PT) injection of electrons from interface states into the conduction band of the phosphor. The total emission rate at an insulator-phosphor interface is the sum of the three separate emission rates:

$$e_n = e_n^{PT} + e_n^{thermal} + e_n^{PAT}. \tag{18}$$

Computation of the separate emission rates for thermal emission, phonon-assisted tunneling, and pure tunneling is performed using analytical forms reported in the literature.[20–22] Then with the total emission rate established, the time rate of change of the charge on an interface is given by

$$\frac{dq_x}{dt} = -e_n[qN_0f_0 - q_x(t)], \tag{19}$$

where N_0f_0 is the no-field occupancy of the interface in question, $q_x(t)$ is the charge on interface x at time t, and e_n is the emission rate computed from Eq. (18). The expressions employed for computation of e_n^{PT}, $e_n^{thermal}$, and e_n^{PAT} are given in Appendix A along with a derivation of Eq. (19).

B. Space-charge creation

The remaining current term to be accounted for is the space-charge current term, $\partial q_{sc}/\partial t$. This term can be modeled

in one of two ways depending on whether it is assumed that space charge is created by impact ionization of deep-level traps or by field emission from states in the band gap of the phosphor layer.

1. Space-charge creation by impact ionization

Impact ionization processes in a semiconductor are generally described by a field-dependent ionization function representing the number of impact ionization events per unit length. To achieve a more practical measure of impact ionization events in a semiconductor in terms of externally measured quantities, the ionization function is manipulated to obtain a multiplication factor across the region of interest. The creation of space charge by impact ionization of deep-level traps is described by an ionization function of the form

$$\alpha_{trap}(f_p) = \left(\frac{n_T}{N_t}\right) \frac{qf_p}{E_{ion}} \exp\left[-\left(\frac{f_0}{f_p}\right)^n\right], \quad n = 1,2, \tag{20}$$

where n_T is the density of traps containing electrons, N_t is the total density of traps in the phosphor, E_{ion} is an effective ionization energy, and f_0 is the characteristic field. For simulation of the single-sheet charge model, an ionization function is computed for both regions of the phosphor, and the relevant field, f_{p1} or f_{p2}, is inserted into Eq. (20). Then, using the two ionization functions computed from Eq. (20), a multiplication factor across the phosphor layer is defined as

$$M_{trap}(f_{p1}, f_{p2}) = \exp[\alpha_{trap}(f_{p1})d_s + \alpha_{trap}(f_{p2})(d_p - d_s)]. \tag{21}$$

Finally, the time rate of change of space charge, $\partial q_{sc}/\partial t$, is computed from

$$\frac{\partial q_{sc}}{\partial t} = J_n(0,t)[M_{trap}(f_{p1}, f_{p2}) - 1], \tag{22}$$

where $J_n(0,t)$ is the electron current emission from the cathodic interface. It should be noted that the derivation of Eqs. (20) through (22) is presented in Appendix B.

In summary, Eqs. (20) through (22) are used to model deep-level trap impact ionization. Note that the amount of deep-level impact ionization is determined by assuming that it occurs throughout the phosphor. However, once the amount of trap ionization is determined, it is assumed to occur exclusively at the single sheet of charge. This methodology is consistent with the philosophy of the single-sheet charge model, which implicitly assumes that a charge distribution may be approximated as a single sheet which represents the charge centroid of the actual charge distribution.

2. Space-charge creation by field emission

The second mechanism for space-charge creation, field emission from traps in the bulk phosphor, is described in an analogous manner to interface emission. The general equations for field emission from a space-charge layer are identical to those for field emission from an interface. However, the depth of the bulk traps and the number of trapped electrons is not, in general, equal to the values for the interfaces. Therefore, the space-charge layer is simply treated as a third interface located in the bulk phosphor layer.

C. Band-to-band impact ionization

In the range of phosphor fields at which ACTFEL devices operate, electron multiplication by band-to-band impact ionization is a distinct possibility. An often-used form for the ionization function,[4]

$$\alpha_{\text{band}}(f_p) = \frac{qf_p}{E_{\text{ion}}} \exp\left[-\left(\frac{f_0}{f_p}\right)^n\right], \quad n = 1,2, \quad (23)$$

is employed for this simulation. In the above equation, E_{ion} is an effective ionization energy and f_0 is a constant that sets the field range where band-to-band impact ionization becomes important. Once again, since the focus of this paper is phosphor space charge, the multiplication factor associated with band-to-band impact ionization cannot be computed using a constant field assumption. Therefore, the formulation of Eq. (21) is used for the multiplication factor due to band-to-band impact ionization with the α_{trap} terms replaced by α_{band} terms. Finally, the additional currents at the interfaces due to band-to-band impaction ionization are computed similar to the time rate of change of space charge in Eq. (22), except that the band-to-band multiplication factor is used. It should also be noted that the holes generated by the band-to-band process are assumed to drift to the cathodic interface and instantaneously recombine with electrons residing at the cathodic interface in this simulation. This assumption of instantaneous electron-hole recombination is not appropriate for simulation of maximum charge-maximum voltage $(Q_{\text{max}}\text{-}V_{\text{max}})$ characteristics[4,23] but is appropriate for the current purpose of simulating $C\text{-}V$ and $Q\text{-}F_p$ overshoot since recombination does not significantly affect overshoot.

IV. FEEDBACK MECHANISMS OF CARRIER EMISSION

The carrier emission mechanisms previously discussed exhibit a feedback effect such that after carriers are emitted, future emission rates are affected. Each of the methods of carrier emission, interface emission, field emission from bulk traps, impact ionization of bulk traps, and band-to-band impact ionization shows feedback effects of varying degree.

A. Interface emission

It has been established previously that as an ACTFEL device begins conducting charge, the charge that piles up on the interfaces sets up a counterfield that opposes the applied field.[3] This effect limits the field in the phosphor layer of the ACTFEL device and can give rise to the so-called field-clamping effect seen in devices not exhibiting space-charge effects. A pictorial representation of the feedback effect of interface emission is illustrated in Fig. 5. As shown in Fig. 5, the applied voltage v_g results in a field across the phosphor layer which causes electron emission from insulator-phosphor interface 1. Electrons emitted from interface 1 drift across the phosphor layer and are collected at interface 2. Continued emission from interface 1 leads to a net negative charge on interface 2, and a net positive charge on interface 1. The charge present at the two interfaces gives rise to the counterfield that reduces the net field across the entire phosphor layer. This self-limiting effect concomitant with inter-
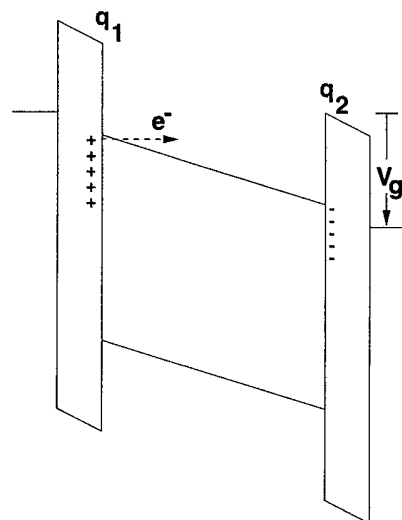

FIG. 5. Interface feedback in ACTFEL devices.

face emission can be viewed as a negative feedback effect and is the essence of the feedback mechanism for interface emission.

B. Space-charge creation

The effects of the presence of a sheet of space charge on the phosphor field can be seen in Fig. 6; the field is no longer constant across the phosphor layer as it is in the absence of space charge; rather, the phosphor field changes discontinuously across the sheet of space charge. This discontinuous change in the phosphor field across the sheet of charge applies to the creation of space charge either by impact ionization of deep-level traps or by field emission from bulk traps. Differences between the two mechanisms arise due to the manner in which each space-charge creation mechanism reacts to changes in phosphor field due to the presence of bulk space charge, as discussed in the following sections.
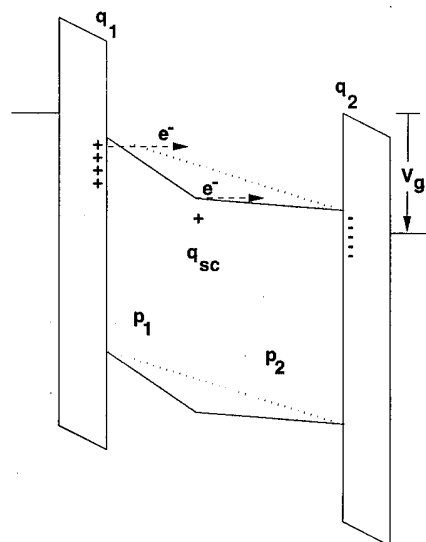

FIG. 6. Phosphor field perturbations caused by the presence of space charge.

1. Impact ionization of deep levels

The creation of space charge by impact ionization of deep-level traps has the weakest feedback effect of the four mechanisms of carrier emission discussed. The feedback effects of carrier emission as space charge is created by impact ionization of deep levels is best described by first considering the effect that space charge has on the phosphor field components and then proceeding from there. As space charge is created by impact ionization of deep levels, the field between the cathodic interface and the sheet of space charge is increased, while the phosphor field between the sheet of space charge and the anodic interface is reduced. These phosphor field perturbations due to the creation of space charge lead to increased electron emission from and trap ionization near the cathodic interface. Similarly, the reduced field near the anodic interface results in decreased deep-level impact ionization in this low-field region. Overall, however, the creation of space charge by impact ionization of deep levels is not a self-limiting process in terms of field feedback. In fact, the feedback in this situation can be positive due to the increased interface emission and the increased ionization rate in the phosphor region near the cathodic interface. Fortunately, the interface feedback effect helps this process from running away by reduction of the field across the entire phosphor with the pileup of charge at the interfaces. However, the effect that limits the creation of space charge by impact ionization of deep levels is the finite number of traps available for ionization within the phosphor layer.

2. Field emission from bulk traps

When space charge is created by field emission from bulk traps, the phosphor fields on either side of the space-charge layer are affected in a manner similar to space-charge creation by impact ionization of deep levels. The similarity arises because the creation of space charge increases the electric field between the cathodic interface and the space-charge layer while the field between the space-charge layer and the anodic interface is reduced. When space charge is created by field emission from bulk traps, bulk emission of electrons is dependent only on the field between the space-charge layer and the anodic interface. This gives rise to a negative feedback effect when space charge is created by field emission because the emission of electrons from the space-charge layer reduces the field that future emission from the space-charge layer is dependent on. Also, the increased field near the cathodic interface causes increased emission from the cathodic interface, which consequently increases the counterfield across the entire device, as discussed in the interface emission feedback section.

C. Band-to-band impact ionization

The mechanism with the strongest feedback effect is band-to-band impact ionization. The exponential rise of the multiplication factor as a function of field can provide a very large electron current to the anodic interface along with a large hole current to the cathodic interface. The operation of the feedback effect associated with band-to-band impact ionization is similar to the feedback effect of interface emission in that the carriers that are emitted produce a counterfield across the entire thickness of the phosphor layer opposing the applied field. However, the large multiplication associated with band-to-band impact ionization can provide many times the number of carriers emitted from the interfaces and, hence, a much stronger feedback effect than interface emission due to the sheer number of carriers involved. Furthermore, the band-to-band impact ionization mechanism can be a major factor in keeping space-charge creation by impact ionization of deep levels at a steady level.

V. ELECTRICAL CHARACTERIZATION OF ACTFEL DEVICES

The focus of this paper is the inclusion of bulk space-charge generation into the standard ACTFEL device model to assess its impact on a device's C-V and Q-F_p characteristics. However, several issues need to be clarified about the actual C-V and Q-F_p measurements themselves in relation to space charge.

A. C-V analysis with space charge

A C-V measurement is performed by monitoring the current through the ACTFEL device during the rising edge of the applied voltage waveform. Then, the measured capacitance of the ACTFEL device is determined[14] by the relation

$$C_m = \frac{i(t)}{\partial v_g / \partial t}. \tag{24}$$

However, the quantity $i(t)$ is known in terms of the single-sheet charge model as $\partial q_e / \partial t$. Therefore, when Eq. (12) is inserted into Eq. (24), an expression for the measured device capacitance in terms of the single-sheet charge model emerges,

$$C_m = \frac{c_i}{c_i + c_p} \left[\frac{\partial q_1}{\partial v_g} + \left(1 - \frac{d_s}{d_p}\right) \frac{\partial q_{sc}}{\partial v_g} \right] + c_t. \tag{25}$$

The above equation shows that space-charge creation adds to the measured capacitance through the $\partial q_{sc}/\partial v_g$ term and is the mechanism responsible for C-V overshoot. Note that Eq. (25) indicates that the location where the space charge is generated also determines the magnitude of the C-V overshoot; the maximum C-V overshoot will occur when the sheet of charge is located near the cathodic interface.

B. Q-F_p analysis with space charge

Recently, the Q-F_p technique has been demonstrated to be a useful electrical measurement for ACTFEL device characterization.[13–15,24] However, Q-F_p analysis implicitly assumes that no space charge exists in the ACTFEL phosphor layer and, thus, that the electric field is constant across the phosphor layer.[3] Since this is not always a reasonable assumption, it needs to be determined what is being measured by this technique when space charge is present in the phosphor. Thus the purpose of this section of the paper is to determine what $q_{int}(t)$ and $f_p(t)$ in a Q-F_p measurement actually represent when space charge is present in the phosphor layer.

J. Appl. Phys., Vol. 78, No. 7, 1 October 1995

Keir, Ang, and Wager   4673

A Q-F_p curve is created by plotting the following expression:

$$q_{int}(t) = \frac{c_i + c_p}{c_i} q_e(t) - c_p v_g(t) \qquad (26)$$

versus

$$f_p(t) = \frac{1}{d_p}\left[\frac{q_e(t)}{c_i} - v_g(t)\right]. \qquad (27)$$

From the above equations, it is seen that the measurable quantities $q_e(t)$ and $v_g(t)$ are needed to compute the quantities $q_{int}(t)$ and $f_p(t)$. Therefore, to determine what is being measured when these quantities are plotted against one another (within the framework of the single-sheet charge model), it is necessary to solve Eqs. (1) through (6) for the quantities on the right-hand sides of Eqs. (26) and (27).

To accomplish this, the right-hand side of Eq. (27) is first solved to determine what $f_p(t)$ represents in a device containing a sheet of space charge. For an ACTFEL device with identical insulating layers, it is known that

$$c_{i1}d_{i1}f_{i1}(t) = c_{i2}d_{i2}f_{i2}(t) = -q_e(t). \qquad (28)$$

For an ACTFEL device, the series combination of the insulator capacitances leads to the total insulator capacitance. Therefore, for an ACTFEL device with identical insulating layers,

$$c_{i1} = c_{i2} = 2c_i, \qquad (29)$$

where c_i is the insulator capacitance. Plugging the above equation into Eq. (7), it is found that

$$d_{i1}f_{i1}(t) = d_{i2}f_{i2}(t) = -\frac{q_e(t)}{2c_i}. \qquad (30)$$

Then, the above equation is substituted into Eq. (1) to yield

$$-\frac{q_e(t)}{c_i} + d_s f_{p1}(t) + f_{p2}(t)(d_p - d_s) = -v_g(t). \qquad (31)$$

Rearranging the above equation, it is found that

$$\frac{d_s}{d_p}f_{p1}(t) + \left(1 - \frac{d_s}{d_p}\right)f_{p2}(t) = \frac{1}{d_p}\left[\frac{q_e(t)}{c_i} - v_g(t)\right], \qquad (32)$$

as desired. Comparing the right-hand side of Eq. (32) to Eq. (27), it is seen that the actual quantity measured for the phosphor field when a Q-F_p measurement is performed is the average phosphor field. This result is derived from the single-sheet charge model, but it can be shown inductively that for n layers of sheet charge the result obtained in the average field is still what is measured.

Next, it is necessary to determine what the q_{int} term in the Q-F_p plot represents when space charge is present in the phosphor layer. To determine this in terms of the single-sheet charge model, it is necessary to solve for the right-hand side of Eq. (26) using Eqs. (1) through (6). Rearranging Eq. (32), it is found that

$$c_p d_p f_{p2}(t) = \frac{c_p q_e(t)}{c_i} - c_p v_g(t) - c_p d_s [f_{p1}(t) - f_{p2}(t)]. \qquad (33)$$

From Eqs. (4) and (5), it is determined that

$$c_p d_p f_{p2}(t) = -q_2(t) - q_e(t). \qquad (34)$$

Then, substitution of the above equation and Eq. (3) into Eq. (32) yields

$$-q_2(t) + \frac{d_s}{d_p} q_{sc}(t) = \frac{c_p + c_i}{c_i} q_e(t) - c_p v_g(t). \qquad (35)$$

Additionally, substitution of the integral of Eq. (12) into the above equation gives $q_{int}(t)$ in terms of $q_1(t)$ and $q_{sc}(t)$, as follows:

$$q_1(t) + \left(1 + \frac{d_s}{d_p}\right)q_{sc}(t) = \frac{c_p + c_i}{c_i} q_e(t) - c_p v_g(t). \qquad (36)$$

Therefore, a comparison of Eqs. (36) and (26) shows that the internal charge measured in a Q-F_p plot of a sample exhibiting space-charge effects is equal to the actual internal charge plus a factor which depends on both the amount and the location of the space charge in the phosphor layer.

VI. SIMULATION IMPLEMENTATION

The ACTFEL device modeling simulation results are obtained from a realization of the single-sheet charge model written in the C programming language. The simulation results are obtained from a numerical solution of Eqs. (13) and (14) with a fourth/fifth order Runge-Kutta-Fehlberg algorithm. All simulations are written and performed using a Hewlett-Packard 9000 type computer. Simulation of ten periods of a 1 kHz driving waveform takes between 15 s and 2 min, depending on the program being run and system usage.

The parameters used in the simulations are listed in Table I. It should be noted that the parameters E_{ion}, E_{ion}^t, N_t, F_0, and F_0^t apply only to the simulation that assumes space-charge creation by impact ionization. Similarly, the parameters $N_0 f_0(sc)$ and E_{sc} apply only to the simulation that assumes space charge creation by field emission from bulk traps. The remaining parameters apply to both types of simulation. Finally, the "n" term in Eqs. (19) and (22) is assumed to be unity for fields below the field threshold, and two for fields above this threshold,[25] where f_0 in Eqs. (19) and (22) is taken to be the threshold field.

The simulation is performed for the case of aluminum-titanium oxide (ATO) insulating layers, and a ZnS:Mn phosphor layer. The dielectric constants of these materials are used in conjunction with the thicknesses of each layer of the ACTFEL device to determine the capacitance of each layer. The thicknesses of each layer are chosen to correspond to the devices tested by Abu-Dayah et al.[14]

VII. RESULTS AND DISCUSSION

A. The origins of C-V and Q-F_p overshoot

One of the primary motivating issues for undertaking the work presented herein is the determination of the origins of C-V and Q-F_p overshoot. First, consider a C-V measurement of an ACTFEL device. The measurement is performed by measuring the instantaneous current through the ACTFEL device and dividing this value by the time rate of change of

TABLE I. Nominal parameter values used for implementing the single-sheet charge model.

Parameter	Description	Nominal parameter value
d_{i1}	Thickness of insulator 1	2700 Å
d_{i2}	Thickness of insulator 2	2700 Å
d_p	Thickness of phosphor layer	5500 Å
d_s	Space-charge location	3500 Å
$N_0 f_0(ip)$	No-field interface occupation	5×10^{13} cm^{-2}
N_t	Bulk trap concentration	1×10^{17} cm^{-3}
$sccf$	Space-charge capture probability	0.1
E_{it}	Interface trap depth	1.0 eV
$N_0 f_0(sc)$	No-field space charge occupation	1×10^{12} cm^{-2}
E_{sc}	Space-charge trap depth	0.9 eV
E_{ion}	Band-to-band effective ionization energy	5.4 eV
E_{ion}^t	Trap-to-band effective ionization energy	2.6 eV
F_0	Band-to-band characteristic field	1.7 MV/cm
F_0^t	Trap-to-band characteristic field	3.0 MV/cm

the voltage dropped across the ACTFEL device. When space charge is being created in the ACTFEL device it perturbs the measured current as seen in Eqs. (12) and (25), so that a capacitance greater than the insulator capacitance may be observed near turn-on. However, as discussed in the section on feedback effects of space charge, space-charge emission occurs such that the creation of space charge tends to turn itself off. Therefore, as the rate of space-charge creation falls towards zero above turn-on, the measured current falls to a level close to what would be measured if no space charge is present. Hence, this produces overshoot in the C-V characteristic of an ACTFEL device with space charge present in the phosphor.

The issue of field overshoot in Q-F_p plots presents another puzzling problem without the inclusion of space-charge effects. The origins of field overshoot in Q-F_p plots is similar in nature to the overshoot in C-V plots, but relates to a different measured quantity. The field overshoot in a Q-F_p plot arises due to the fact that the F_p measured in a Q-F_p plot is actually the average phosphor field. The reason that overshoot is seen is that the average phosphor field is at first a certain value that is then reduced after space-charge creation begins. This can again be traced to the feedback effect of space-charge creation.

B. Impact ionization

Simulation of space charge in the phosphor layer by impact ionization of deep-level impurities shows several interesting effects. First, the addition of band-to-band impact ionization to the simulation along with impact ionization of traps leads to a significantly larger overshoot in both the C-V and Q-F_p plots than when only impact ionization of traps is included. A comparison of simulated C-V plots both with and without band-to-band impact ionization is given in Fig. 7.

It is established in Eq. (24) that the magnitude of the C-V overshoot is a function of the location of the space-charge layer and the partial derivative of the amount of space charge with respect to the applied voltage. In steady state, the amount of space charge generated during one period of the driving waveform is equal to the amount of space charge

annihilated during the period. Therefore, when band-to-band impact ionization is included in the simulation along with impact ionization of traps, there is a significantly larger amount of charge transferred to the insulator-phosphor interfaces. This increase in charge on the interfaces leads to a larger amount of charge transferred during the interpulse interval or low-field portion of the driving waveform. The larger amount of charge transfer during the interpulse interval leads to a greater amount of space-charge annihilation, and hence, a greater overshoot because the amount of space charge annihilated in one period must equal the amount of space charge generated in steady state.

A simulated Q-F_p plot with both band-to-band and deep-level impact ionization included and a simulated Q-F_p plot without bulk space charge are shown in Fig. 8. Figure 8 shows that space-charge creation by impact ionization causes the average phosphor field for different polarity pulses to be quite different. In contrast, the simulated Q-F_p curve without space charge included in the phosphor layer shows that the field for both polarity pulses is approximately equal. Also, Fig. 8 shows that more charge is transferred across the phosphor layer when space charge is present, as would be expected intuitively. Finally, Fig. 8 shows that the Q-F_p curve is shifted so it is no longer centered around the point
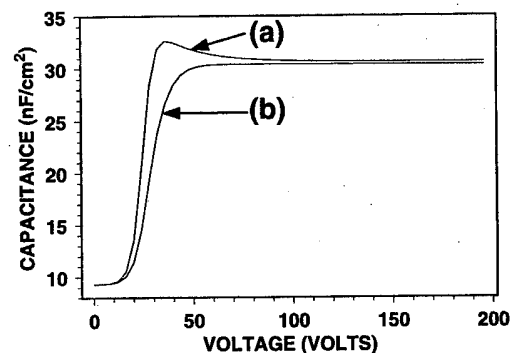

FIG. 7. Simulated Al− C-V plots of an ACTFEL device with (a) both impact ionization of deep-level traps and band-to-band impact ionization included and (b) only impact ionization of deep-level traps included.
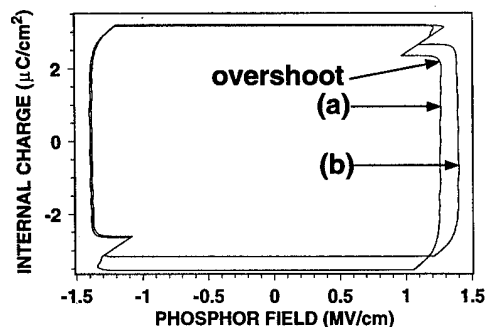
FIG. 8. Simulated Q-F_p plots of an ACTFEL device with (a) both impact ionization of deep-level traps and band-to-band impact ionization included and (b) impact ionization of traps not included.

FIG. 10. Simulated C-V plot of an ACTFEL device without space charge in the phosphor layer.

where the internal charge and the phosphor field are zero when space-charge creation is included.

C. Field emission

The creation of space charge by field emission from bulk traps is the second type of single-sheet charge model simulated. As is the case of deep level plus band-to-band impact ionization, the creation of space charge by field emission causes both C-V and Q-F_p overshoot. However, for space-charge creation by field emission it is not necessary to have band-to-band impact ionization present in order to observe field overshoot. This is due to the fact that space-charge creation by field emission effectively limits itself, as discussed in the section on feedback effects of space-charge creation.

The simulated results for space-charge creation by field emission are very similar to those simulated assuming impact ionization; this can be seen by comparing the C-V plots of space-charge creation by field emission shown in Fig. 9 to the corresponding plots for impact ionization in Fig. 7. It should be noted that the device structures for both the field emission and the impact ionization simulations shown in Figs. 7 and 9 are identical. Furthermore, the space-charge layer is located at the same position in the phosphor layer for both simulations. For comparison purposes, a simulated C-V plot without any space charge is shown in Fig. 10. The relevance of this plot is that exactly the same parameters are
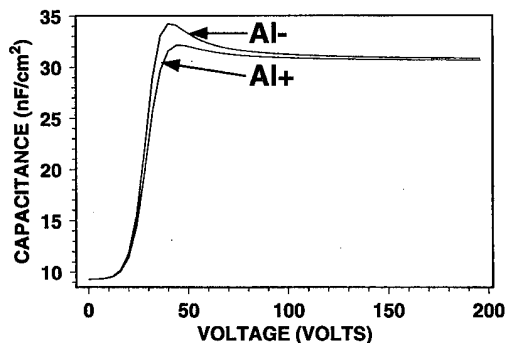
used for the simulations shown in Figs. 9 and 10. However, as seen, the presence of space charge in the phosphor leads to a C-V response exhibiting overshoot.

A Q-F_p plot with bulk space charge created by field emission is shown in Fig. 11. It is seen in Fig. 11 that there is again a small field overshoot for one field polarity, as is the case for space charge created by impact ionization. Furthermore, the maximum average phosphor fields shown in the Q-F_p plot are again different for each polarity of field. Also, it is seen that space-charge creation by field emission makes the Q-F_p plot asymmetrical about the line where internal charge is zero. Furthermore, it is seen that the Q-F_p plot of an ACTFEL device without space charge present in the phosphor layer exhibits symmetry about the line where the internal charge is zero. The result of these asymmetries is that the Q-F_p plot is offset so that the center of the Q-F_p curve is no longer the point where both the internal charge and the phosphor field are zero, as it is in the Q-F_p curve for an ACTFEL device with no space charge in the phosphor. It is interesting to note that a similar offset of internal charge is not seen in the case of space-charge creation by impact ionization of deep-level traps, as evident in Fig. 8.

D. Space-charge parameter variation trends

As mentioned previously, the parameters used in the simulation of Figs. 7 and 10 are collected in Table I. The purpose of the following subsection is to explore simulation

FIG. 9. Simulated C-V plots of both polarity pulses for an ACTFEL device with a space-charge layer at d_s=3500 Å which is created by field emission.
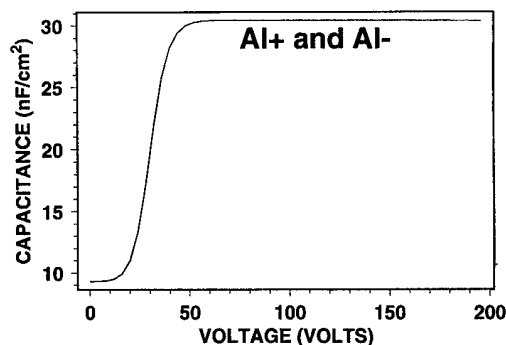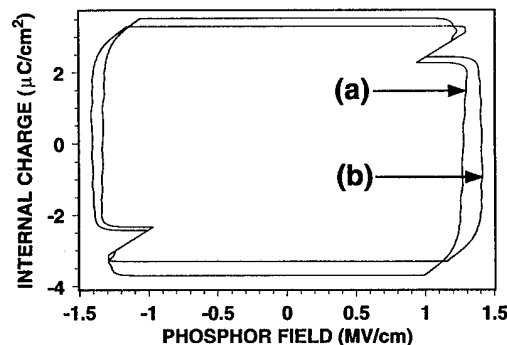

FIG. 11. Simulated Q-F_p plots of an ACTFEL device with (a) a layer of space charge at d_s=3500 Å created by field emission and (b) no space charge in the phosphor layer.
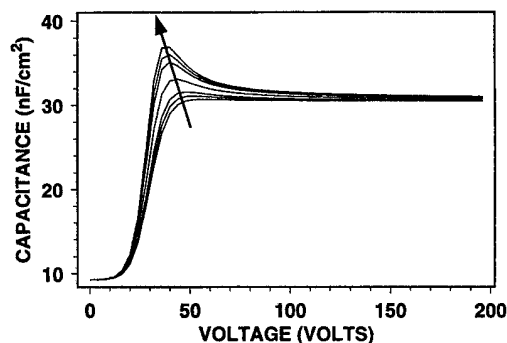
Keir, Ang, and Wager

FIG. 12. Family of C-V curves for Al$-$ (the arrow indicates increasing d_s; d_s=500, 1000, 1500, 2750, 4000, 4500, and 5000 Å).

FIG. 14. Family of Q-F_p curves representing changing d_s (the arrow indicates increasing d_s; d_s=500, 2750, and 5000 Å).

trends when the magnitudes of some of the key simulation parameters are systematically varied. It should be noted that the following discussions of variations of space-charge parameters assume the device structure of Fig. 1, where V_g is applied to an Al electrode and the indium tin oxide (ITO) electrode is grounded.

1. Trends when d_s is varied

The results of a parametric variation of d_s, the location of the space-charge layer, on the C-V plots of both polarities is provided in Figs. 12 and 13. As seen in these figures, the location of the space charge has a very important effect on the magnitude of the overshoot seen in the C-V plot. Also, the location of the space charge determines the polarity of the pulse for which overshoot is witnessed. For example, the family of C-V plots shown in Fig. 12 demonstrates that the overshoot of a negative polarity pulse increases as the space-charge layer nears the insulator-phosphor interface on the ITO side of the device. Similarly, Fig. 13 shows that the overshoot exhibited in a C-V curve from a positive applied pulse decreases as the space-charge centroid moves closer to the insulator- phosphor interface on the ITO side of the device. This trend is actually predicted by Eq. (25) which shows that the C-V overshoot term is actually the product of $\partial q_{sc}/\partial v_g$ and the location dependent term, $1-(d_s/d_p)$.

A similar trend is apparent for the family of Q-F_p plots shown in Fig. 14. As the space-charge layer moves close to one interface, the overshoot observed is very asymmetrical in
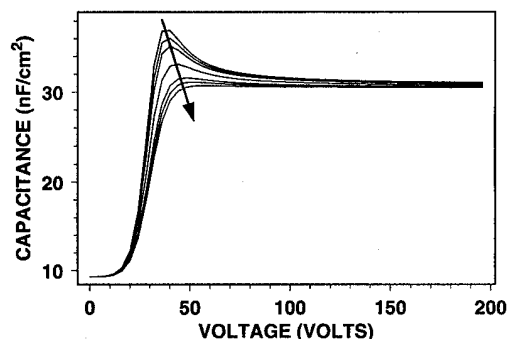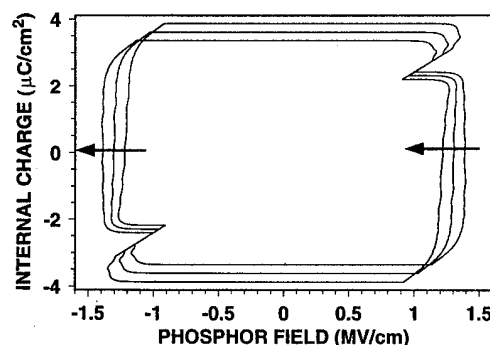
that it is seen for only one polarity pulse. This asymmetry appears near both the far left and right side of the Q-F_p plot and the arrows mark increasing d_s. Therefore, for a laboratory measurement, the location of the space charge in the phosphor layer can be roughly determined by examining the asymmetry in the overshoot characteristics and comparing it to simulated results.

Comparison of the simulated results shown in Figs. 12 and 13 with the results from experiments performed[13,14] on ALE ZnS:Mn devices by Abu-Dayah et al. shed some light on the location of the space-charge layer in these devices. Figure 13 shows that small or no overshoot is seen for an Al$+$ C-V measurement when the space-charge layer is located near the insulator-phosphor interface on the Al side of the device. Alternately, Fig. 12 shows that a large overshoot is produced for an Al$-$ C-V measurement when the space-charge layer is located near the insulator-phosphor interface on the ITO side of the ACTFEL device. When Figs. 12 and 13 are compared with the experimental results of Abu-Dayah et al.,[13] it is seen that the experimental results are very similar to the simulated results when the sheet of space charge is located very near the insulator-phosphor interface on the Al side of the device. Thus, the simulated results provide evidence that the centroid of the space-charge distribution for the ACTFEL device samples used for the study by Abu-Dayah et al. lies near the insulator-phosphor interface on the Al side of the device; this result is in contrast to previous conclusions of Douglas et al.[26] and Abu-Dayah et al.[13,14] who asserted that space-charge creation occurs near the bottom, ITO interface.

2. Trends exhibited with variation of capture efficiency

Another space-charge simulation parameter is the space-charge capture efficiency. Presently, the simulation assumes that a negligible amount of space charge is annihilated during the application of voltage pulses to the ACTFEL device. However, in the interpulse interval it is assumed that space charge is likely to be annihilated and can be described by a capture ratio that determines what percentage of the charge transferred during the interpulse interval annihilates space charge. This assumption is made because prior researchers have shown that the capture cross section for space-charge
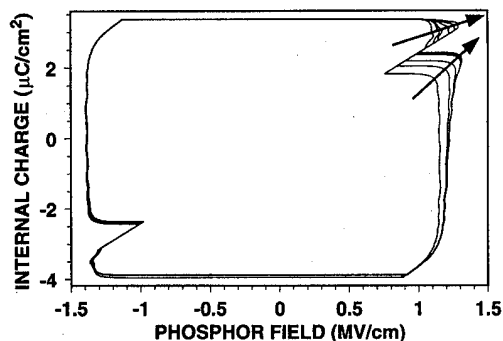

FIG. 13. Family of C-V curves for Al$+$ (the arrow indicates increasing d_s; d_s=500, 1000, 1500, 2750, 4000, 4500, and 5000 Å).

J. Appl. Phys., Vol. 78, No. 7, 1 October 1995

Keir, Ang, and Wager   4677

FIG. 15. Family of Q-F_p curves representing a variation of the bulk trap capture efficiency (the arrows indicate increasing capture efficiency; sccf =0.01, 0.05, 0.1, 0.3, 0.5, 0.7).

capture processes decreases rapidly with field.[27] Therefore, during the high-field portion of the operation of the ACTFEL device it is assumed that the amount of electron capture by the space-charge layer is negligible.

According to simulated results this capture ratio for space-charge annihilation is a very important parameter. The results of several simulations which show the effects of this parameter are illustrated in Fig. 15. These simulations show that as space-charge capture becomes more efficient, the device exhibits increasing overshoot. Also, as capture becomes more efficient, the interpulse leakage charge is reduced. The basic reasoning behind this effect is once again related to the amount of space charge being constant at points in time separated by one period of the driving waveform. This means that as the space charge becomes more efficient at charge capture during the low-field portion of the pulse, more space charge that will be annihilated. However, because the device is in steady state, the amount of space charge annihilated during the interpulse interval must equal the amount of space charge created during the pulse. Therefore, greater overshoot is witnessed in accordance with Eq. (25). This result leads to the conclusion that it is not the presence of space charge in the phosphor layer that causes many of the effects attributed to space charge, but the interaction between the charge at the sheet of space charge and at the insulator-phosphor interfaces.

VIII. CONCLUSIONS

Simulation of space charge in the phosphor layer of an ACTFEL device using a single-sheet charge model provides evidence that space-charge creation is indeed responsible for C-V and Q-F_p overshoot. Specifically, Figs. 7 and 10 show that space-charge creation by either impact ionization of deep-level traps or by field emission from bulk traps causes overshoot in C-V measurements of ACTFEL devices. In addition, simulated Q-F_p overshoot is seen in Figs. 8, 11, 14, and 15. Furthermore, the amount of overshoot exhibited by a sample is dependent on several parameters such as the location of the space charge in the phosphor layer and the capture efficiency of the bulk traps. The amount of overshoot exhibited by a sample also depends on the polarity of the applied voltage pulse. As shown in Fig. 10, C-V plots for different polarities of the applied voltage can exhibit vastly different overshoot characteristics.

The simulation of space charge in the phosphor layer using a single-sheet charge model has indicated that a space-charge distribution with a centroid near one of the insulator-phosphor interfaces causes the asymmetrical overshoot characteristics witnessed in Fig. 9 and experimental work.[13–15] From the overshoot characteristics of two different polarity C-V plots for a given ACTFEL device sample, a rough estimate of the location of the centroid of the space-charge distribution in the phosphor layer can be determined using the simulated data given in Figs. 12 and 13. Also, the amount of overshoot and the leakage charge exhibited by a sample has been shown to be dependent on the capture efficiency of the charged bulk phosphor layer traps. However, the capture efficiency does not show any effects related to applied voltage polarity, as does the location of the space-charge layer.

APPENDIX A: INTERFACE EMISSION RATES

The expression for the emission rate due to pure tunneling from a discrete Coulombic well e_n^{PT} is[20–22]

$$e_n^{PT}(f_p) = \frac{qf_p}{4(2m^*E_{it})^{1/2}} \exp\left\{\left(-\frac{4}{3}\frac{(2m^*)^{1/2}E_{it}^{3/2}}{q\hbar f_p}\right)\right.$$

$$\left.\times\left[1-\left(\frac{\Delta E_{it}}{E_{it}}\right)^{5/3}\right]\right\}, \tag{A1}$$

where E_{it} is the depth of the discrete interfacial trap and

$$\Delta E_{it} = q\left(\frac{qf_p}{\pi\epsilon_p}\right)^{1/2}. \tag{A2}$$

Next, the thermal emission rate from a discrete trap, $e_n^{thermal}$, is given by[21]

$$e_n^{thermal}(f_p) = \sigma v_{th}N_c \exp\left(-\frac{E_{it}-\Delta E_{it}}{kT}\right), \tag{A3}$$

where k is Boltzmann's constant, T is the temperature in degrees Kelvin, σ is the capture cross section for thermal emission, N_c is the effective density of states, and v_{th} is the thermal velocity. Finally, the emission rate due to phonon-assisted tunneling from a discrete trap, e_n^{PAT}, is given by[20–22]

$$e_n^{PAT} = e_n^{thermal}\int_{\Delta E_{it}/kT}^{E_{it}/kT}\exp\left[z-z^{3/2}\left(\frac{4}{3}\frac{(2m^*)^{1/2}(kT)^{3/2}}{q\hbar f_p}\right)\right.$$

$$\left.\times\left(1-\left(\frac{\Delta E_{it}}{zkT}\right)^{5/3}\right)\right]dz. \tag{A4}$$

4678   J. Appl. Phys., Vol. 78, No. 7, 1 October 1995

Keir, Ang, and Wager

These emission rates given by Eqs. (A1), (A3), and (A4) are then inserted into Eq. (18) to yield the total emission rate of the interface.

The time rate of change of $q_x(t)$, the charge on interface x at time t, is

$$\frac{dq_x}{dt} = -qe_n n_x(t), \tag{A5}$$

where $n_x(t)$ is the number of electrons present at interface x at time t. The expression for the charge at an interface in terms of $n(t)$ is given by[3]

$$q_x(t) = q[N_0 f_0 - n_x(t)], \tag{A6}$$

where $N_0 f_0$ is the no-field occupancy of the interface in question. Hence, solving for $n_x(t)$ in the above equation and substituting into Eq. (A5) yields

$$\frac{dq_x}{dt} = -e_n[qN_0 f_0 - q_x(t)], \tag{A7}$$

where $q_x(t)$ can be found in terms of the phosphor fields using Eqs. (1) through (6).

APPENDIX B: IMPACT IONIZATION OF DEEP-LEVEL TRAPS

The impact ionization of deep-level traps in a semiconductor has been shown to be fit by ionization functions of the form[25]

$$\alpha_{\text{trap}}(f_p) = B(f_p)\exp\left[-\left(\frac{f_0}{f_p}\right)^n\right], \quad n=1,2. \tag{B1}$$

Also, the ionization function, $\alpha_{\text{trap}}(f_p)$ is often expressed[25,28]

$$\alpha_{\text{trap}}(f_p) = N_t \sigma(f_p), \tag{B2}$$

where $\sigma(f_p)$ is the capture cross section for the process and N_t is the trap density in the semiconductor. A common field-dependent form for the ionization function multiplier, $B(f_p)$, is[4]

$$B(f_p) = \frac{qf_p}{E_{\text{ion}}}. \tag{B3}$$

If Eqs. (B1) and (B3) are used to determine the ionization function, the cross section for the process, $\sigma(f_p)$ can be found by equating the ionization function determined by Eqs. (B1) and (B3) to that in Eq. (B2). This results in

$$\sigma(f_p) = \frac{\alpha_{\text{trap}}(f_p)}{N_t} = \frac{qf_p}{N_t E_{\text{ion}}}\exp\left[-\left(\frac{f_0}{f_p}\right)^n\right], \quad n=1,2. \tag{B4}$$

However, Eq. (B4) refers to a situation in which all of the traps are filled with electrons and, hence, N_t trapped electrons are always available to be promoted to the conduction band. Since it is assumed that the impact ionization process creates space charge in the phosphor layer, there is a reduction in the number of traps available for ionization as traps become ionized. Therefore, the quantity n_T, the density of traps containing electrons, must be introduced into Eq. (B4) to obtain the final expression for the impact ionization function,

$$\alpha_{\text{trap}}(f_p) = n_T \sigma(f_p) = \left(\frac{n_T}{N_t}\right)\frac{qf_p}{E_{\text{ion}}}\exp\left[-\left(\frac{f_0}{f_p}\right)^n\right], \quad n=1,2. \tag{B5}$$

With the form of the ionization function now established, it is necessary to examine current continuity. Neglecting recombination-generation processes in the phosphor, the current continuity equation for electrons becomes[4]

$$\frac{\partial J_n}{\partial x} = \alpha_{\text{traps}}(f_p)J_n, \tag{B6}$$

which has the solution

$$J_n(x,t) = J_n(0,t)\exp[\alpha_{\text{traps}}(f_p)x]. \tag{B7}$$

However, in the single-sheet charge model it is implicitly assumed that there are two regions of the phosphor layer whose fields are not in general equal. Therefore, it is necessary to examine the current continuity equation in each region separately. First, in region $p1$,

$$\frac{\partial J_n}{\partial x} = \alpha_{\text{traps}}(f_{p1})J_n, \quad 0 \leq x \leq d_s, \tag{B8}$$

meaning that

$$J_n(x,t) = J_n(0,t)\exp[\alpha_{\text{traps}}(f_{p1})x], \quad 0 \leq x \leq d_s. \tag{B9}$$

Similarly, in region $p2$,

$$\frac{\partial J_n}{\partial x} = \alpha_{\text{traps}}(f_{p2})J_n, \quad d_s \leq x \leq d_p, \tag{B10}$$

such that

$$J_n(x,t) = J_n(d_s,t)\exp[\alpha_{\text{traps}}(f_{p2})(x-d_s)], \quad d_s \leq x \leq d_p. \tag{B11}$$

Then, since Eqs. (B9) and (B11) must be equal at d_s, it is determined that

$$J_n(d_s,t) = J_n(0,t)\exp[\alpha_{\text{traps}}(f_{p1})d_s]. \tag{B12}$$

Finally, substituting Eq. (B12) into Eq. (B11) and evaluating the resultant expression at the anodic interface, the current arriving at the anodic interface is determined to be

$$J_n(d_p,t) = J_n(0,t)\exp[\alpha_{\text{traps}}(f_{p1})d_s]$$
$$\times \exp[\alpha_{\text{traps}}(f_{p2})(d_p-d_s)]. \tag{B13}$$

Therefore, the multiplication factor across the entire phosphor is given by

$$M(f_{p1},f_{p2}) = \exp[\alpha_{\text{traps}}(f_{p1})d_s + \alpha_{\text{traps}}(f_{p2})(d_p-d_s)]. \tag{B14}$$

It should be noted that this analysis is only valid for the case where interface 1 is the cathodic interface and interface 2 is the anodic interface (i.e., a positive applied voltage to the A1 contact). However, the analysis for a negative applied voltage proceeds in exactly the same manner, and the same solution is obtained except for the fact that the $J_n(0,t)$ term in Eq. (B13) is replaced by $J_n(0,t)$, so that the details are omitted.

J. Appl. Phys., Vol. 78, No. 7, 1 October 1995

Keir, Ang, and Wager   4679

[1] Y. S. Chen and D. C. Krupka, J. Appl. Phys. **43**, 4089 (1972).

[2] D. H. Smith, J. Lumin. **23**, 209 (1981).

[3] E. Bringuier, J. Appl. Phys. **66**, 1314 (1989).

[4] E. Bringuier, J. Appl. Phys. **67**, 7040 (1990).

[5] K. A. Neyts and P. De Visschere, J. Appl. Phys. **68**, 4163 (1990).

[6] A. A. Douglas and J. F. Wager, SID 92 Digest, 365 (1992).

[7] A. A. Douglas, M. S. thesis, Oregon State University, 1993.

[8] W. E. Howard, J. Lumin. **23**, 155 (1981).

[9] W. E. Howard, O. Sahni, and P. M. Alt, J. Appl. Phys. **53**, 639 (1982).

[10] K. W. Yang and S. J. T. Owen, IEEE Trans. Electron Devices **ED-30**, 452 (1983).

[11] B. K. Ridley and F. A. El-Ela, J. Phys. Condens. Matter **1**, 7021 (1989).

[12] K. A. Neyts, D. Corlatan, P. De Visschere, and J. Van den Bossche, J. Appl. Phys. **75**, 5339 (1994).

[13] A. Abu-Dayah, S. Kobayashi, and J. F. Wager, J. Appl. Phys. **74**, 5575 (1993).

[14] A. Abu-Dayah and J. F. Wager, J. Appl. Phys. **75**, 3593 (1994).

[15] A. Abu-Dayah, S. Kobayashi, and J. F. Wager, Appl. Phys. Lett. **62**, 744 (1993).

[16] J. M. Jarem and V. P. Singh, IEEE Trans. Electron Devices **ED-35**, 1834 (1988).

[17] K. A. Neyts, IEEE Trans. Electron Devices **ED-38**, 2604 (1991).

[18] V. P. Singh, W. Z. Majid, and D. C. Morton, J. SID **1-2**, 135 (1993).

[19] A. Goldenblum, A. Oprea, and V. Bogatu, J. Appl. Phys. **75**, 5177 (1994).

[20] G. Vincent, A. Chantre, and D. Bois, J. Appl. Phys. **50**, 5484 (1979).

[21] E. Rosencher, V. Mosser, and G. Vincent, Phys. Rev. **29**, 1135 (1983).

[22] S. Kobayashi, J. F. Wager, and A. Abu-Dayah, *Electroluminescence*, edited by V. P. Singh and J. C. Mc Clure (Cinco Puntos, El Paso, TX, 1992), p. 234.

[23] W. M. Ang, S. Pennathur, L. Pham, J. F. Wager, S. M. Goodnick, and A. A. Douglas, J. Appl. Phys. **77**, 2719 (1995).

[24] L. V. Pham, J. F. Wager, S. S. Sun, E. Dickey, R. T. Tuenge, and C. N. King, in *Advanced Flat Panel Display Technologies*, edited by P. S. Friedman (SPIE, Bellingham, WA, 1994), Proc. 2174, pp. 190–199.

[25] A. W. Livingstone and J. W. Allen, J. Phys. C **6**, 3491 (1973).

[26] A. A. Douglas, J. F. Wager, D. C. Morton, J. B. Koh, and C. P. Hogh, J. Appl. Phys. **73**, 296 (1993).

[27] D. A. Buchanan, M. V. Fischetti, and D. J. DiMaria, Phys. Rev. B **43**, 1471 (1991).

[28] D. J. Robbins, Phys. Status Solidi **98**, 11 (1980).